Journal of Magnetic Resonance 214 (2012) 76–80

Contents lists available at SciVerse ScienceDirect

Journal of Magnetic Resonance

journal homepage: www.elsevier.com/locate/jmr

A supplementary coil for ^{2}H decoupling with commercial HCN MAS probes

Matthias Huber, Oliver With, Paul Schanda, René Verel, Matthias Ernst, Beat H. Meier *

Physical Chemistry, ETH Zürich, Wolfgang-Pauli-Strasse 10, 8093 Zürich, Switzerland

ARTICLE INFO

Article history:
Received 2 September 2011
Revised 11 October 2011
Available online 20 October 2011

Keywords:
Solid-state NMR spectroscopy
Decoupling
Deuteration
Proton-detection
Probe-design

ABSTRACT

Partial deuteration is a powerful tool to increase coherence life times and spectral resolution in proton solid-state NMR. The J coupling to deuterium needs, however, to be decoupled to maintain the good resolution in the (usually indirect) ^{13}C dimension(s). We present a simple and reversible way to expand a commercial 1.3 mm HCN MAS probe with a ^{2}H channel with sufficient field strength for J-decoupling of deuterium, namely 2–3 kHz. The coil is placed at the outside of the stator and requires no significant modifications to the probe. The performance and the realizable gains in sensitivity and resolution are demonstrated using perdeuterated ubiquitin, with selectively CHD_2-labeled methyl groups.

1. Introduction

While biological solid-state NMR is heavily based on the observation of ^{13}C and ^{15}N spins, proton detection is of increasing interest since the observation of sparsely placed protons in otherwise perdeuterated samples has been demonstrated to lead to highly resolved proton spectra. Such samples can be produced by expression in a mixture of H_2O and D_2O (and perdeuterated glucose) [1], by perdeuteration of the protein and crystallization/fibrillization from a partially protonated buffer [2,3] or, for methyl labelling, through the use of α-ketoacid precursors [4]. All of these approaches yields samples with ^{15}N and/or ^{13}C spins with directly bound ^{2}H spins. As one of many examples $^{13}CHD_2$ labeling of methyl groups has been used to study protein structure [5] and dynamics [6,7]. To obtain sensitive and highly resolved ^{13}C–^{1}H correlation spectra ^{13}C–^{2}H J-decoupling is essential, while the dipolar coupling is sufficiently reduced by the MAS. While some commercial triple resonance probes can be tuned to ^{1}H–^{13}C–^{2}H, many probes for biomolecular NMR are restricted to ^{1}H–^{13}C–^{15}N. In addition, many experiments also require a ^{15}N dimension and therefore a quadruple resonance ^{1}H–^{13}C–^{2}H–^{15}N probe.

Here, we present a way to install an auxiliary ^{2}H coil in a commercial Bruker 1.3 mm HCN probe that does not require significant modification of the existing hardware. We demonstrate on a microcrystalline [U–^{2}H^{15}N; Ile–$^{13}CHD_2$] labelled sample of ubiquitin, that ^{2}H decoupling with such an auxiliary ^{2}H coil greatly enhances sensitivity and resolution of the [^{13}C,^{1}H]-HSQC spectrum.

2. Design considerations

Different considerations guided our design of a ^{2}H coil for J-decoupling purposes. (i) We aim for a supplementary coil which creates a B_1 field of an amplitude such that γB_1 is of the order of several kHz. (ii) The inhomogeneity ΔB_1 should be below 10% over the sample volume which can be easily handled by decoupling sequences [8]. (iii) The rf characteristics of the main coil should remain unchanged, i.e. the coupling of the coils must be minimal. (iv) All modifications to the probe should be simple and completely reversible. This is most easily achieved by placing the auxiliary coil outside the MAS stator.

In order to minimize the coupling between the two coils, we chose for a design where the field generated by the auxiliary coil and the one generated by the main coil, in our case a triply tuned solenoid coil, are perpendicular. Our design resembles a Helmholtz coil but without the condition that the distance between two sets of coils is equal to the coil's radius (see Fig. 1). The field is parallel to the *x*-direction and perpendicular to the one produced by the main coil being at the magic angle in the *yz*-plane. The B_1 field of the ^{2}H coil on the *x*-axis halfways between the two parts of the coils is given by [9]:

$$B_x = \frac{\mu_0 \cdot I_{coil} \cdot n}{2} \cdot \frac{R^2}{\left((D/2)^2 + R^2\right)^{3/2}}. \quad (1)$$

Here, I_{coil} is the current in the coil, n the total number of loops, D the distance between the two sets of loops and R the radius of a loop. The maximum field is produced at $R = D/\sqrt{2}$. The inductance of the structure in Fig. 1 is given by [10]: $L_1, L_2 = (\frac{n_{l,r}}{2})^2 \cdot L_{loop}$ where $n_{l,r}$ is the number of loops per side and $L_{loop} = R \cdot \mu_0 \cdot \left(\ln\frac{4R}{a} - 2\right)$ is

* Corresponding author. Fax: +41 44 632 1621.
E-mail address: beme@ethz.ch (B.H. Meier).
URL: http://www.ssnmr.ethz.ch (B.H. Meier).

1090-7807/$ - see front matter © 2011 Elsevier Inc. All rights reserved.
doi:10.1016/j.jmr.2011.10.010

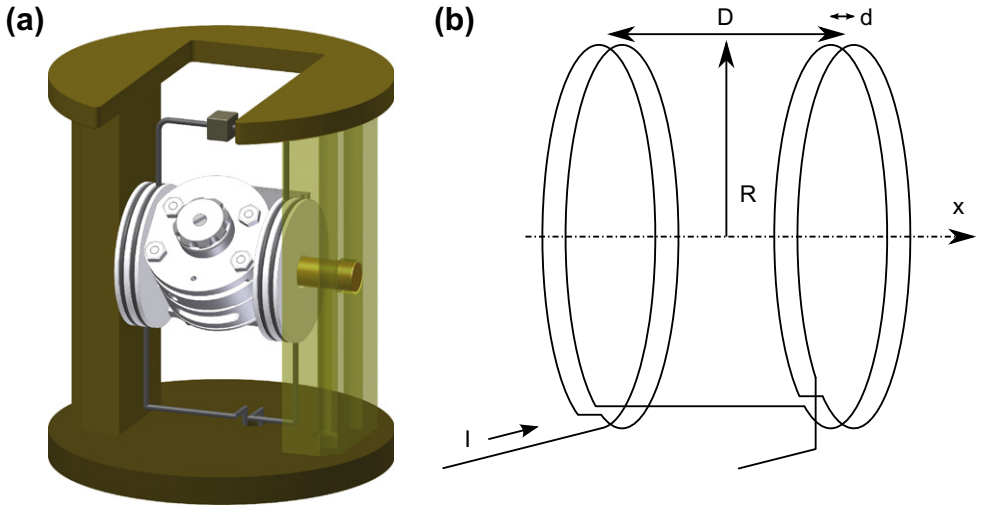

Fig. 1. Geometry and installation of the auxiliary ^{2}H coil. (a) Two loops of the coil are on each side of the MAS stator with a capacitor C_{seg} above. This geometry ensures orthogonality of the fields generated by the two coils. The leads are guided through the bottom plate of the stator chamber, using the preexisting hole for optical spinning control and are connected to the tuning circuit in the lower part of the probe. (b) The ^{2}H coil consists of two solenoids with radius R = 12 mm that are separated form each other by the width of the stator D = 24 mm. Each solenoid is two-turned with a spacing d = 2 mm.

the inductance of a single loop. The wire resistance associated with the coil is calculated by $R_s = \ell \cdot \sqrt{\frac{\omega}{2\sigma\mu_0}} \cdot \frac{1}{\pi a}$ where σ is the conductance and a the diameter of the wire. The main stray capacitance is between the windings of the coil and is calculated by $C_{stray} = \frac{\pi\varepsilon\ell}{\operatorname{acosh}(d/a)}$, where ℓ is the length of two parallel wires and d the distance between the wires (see Fig. 1b). Small stray capacitances also occur between conductors and ground but are difficult to specify in analytical form. These capacitances add onto the tuning capacitor C_T.

Using network theory the steady-state current in the coil of Fig. 2b is calculated as [9]

$$I_{coil} = \frac{2\sqrt{P \cdot R_i}}{(R_i + (i\omega C_T + \frac{1}{Z_{coil}+R_s})^{-1} - \frac{1}{i\omega C_m}) \cdot (i\omega C_T + \frac{1}{Z_{coil}+R_s}) \cdot (Z_{coil} + R_s)} \quad (2)$$

where R_i is the amplifier's internal impedance and P the amplifier's output power.

Since the coil is unusually large, the resulting inductance of L_1, L_2 and the leads is roughly 600 nH. This would lead to a very low value for tuning capacitance C_T. With the stray capacitances between the loops acting as tuning capacitances C_T would be even lower. Therefore the two coils are split with a capacitor C_{seg} to lower the overall impedance of the coil. Furthermore, the tuning capacitance is split into C_{T1} and C_{T2}. The resulting impedance (Z_{coil}) is much lower than the impedance of the coil alone and can be controlled by the choice of C_{seg} and C_{T2}.

$$Z_{coil} = \left(j\omega L_1 + j\omega L_2 + \frac{1}{j\omega C_{seg}} + \frac{1}{j\omega C_{T2}}\right) \quad (3)$$

This balanced circuit (Fig. 2b) has a number of advantages. The influence of stray capacitances to ground is cut in half, the voltages with respect to ground are only half as high and the values of C_{T1} and C_{T2} can be chosen flexibly.

To avoid major modifications to the probe, no rods for tuning from the outside were installed. Therefore C_{T2} can only be adjusted while the probe is outside the magnet and open and the matching capacity C_M has a fixed value. By choosing the matching capacity C_M somewhat larger than optimal we achieve a larger bandwidth while accepting a slight mismatch and reduction of the quality factor Q.

The component's values of the equivalent circuit (Fig. 2) are as follows: L_1 and $L_2 \approx 300$ nH each, C_{T1} = 4.3 pF, C_{T2} = 1 ... 20 pF, C_M = 1.6 pF, C_{seg} = 10 pF, $R_s \approx 0.6\,\Omega$ with $\sigma = 60 \times 10^6$ Sm^{-1}, a = 1 mm, $l \approx 0.5$ m and $R_i = 50\,\Omega$.

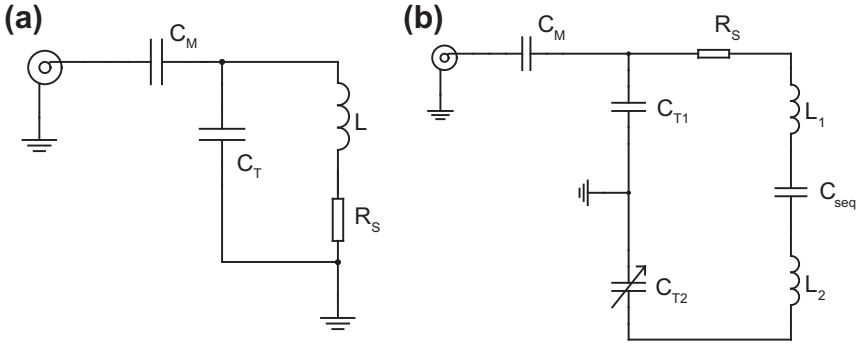

Fig. 2. Schematic diagram of the ^{2}H circuits. (a) Basic tuning single resonance circuit. (b) Circuit used here. To reduce the overall inductance the coil is split into L_1 and L_2 by the segmentation capacitance C_{seg}. The tuning capacitance C_T is split into C_{T1} and C_{T2} to achieve a balanced network. Since no tuning rods are installed C_{T2} can only be adjusted while the probe is outside the magnet. Therefore, we chose the matching capacity C_M slightly larger than optimal to increase the bandwidth. The capacitators used were C_{T1} = 4.3 pF, C_M = 1.6 pF, C_{seg} = 10 pF and C_{T2} tunable 1 ... 20 pF (set to ≈6 pF).

To create an rf-field of 2 kHz amplitude (corresponding to B_1 = 0.612 mT) we need, according to Eq. (1), a current I of approximately 8 A. With Eq. (2) and (3), we can calculate the required power at the amplifier to be ≈100 W.

3. Results and discussion

We tested the performance of the auxiliary coil by recording a nutation curve that permits to extract rf-field strength and homogeneity. We applied a power level of 125 W and pulse durations between 50 μs and 5 ms (Fig. 3a), observing the D_2O resonance of a rotor filled with deuterated ubiquitin to be used later for the protein experiments. The first maximum of the nutation curve occurs at about 125 μs corresponding to a nutation frequency of 2 kHz. The B_1 field distribution in the sample volume is obtained from the Fourier Transformation of the nutation curve. Here an unusual bimodal distribution is observed (Fig. 3c). We performed a finite elements simulation to gain insight into the spatial distribution of the B_1 field. Fig. 3b shows that for the central part of the MAS rotor the ^{2}H field is partly shielded by the inner triple resonance coil, and we can thus ascribe the two components of the rf distribution to parts of the sample inside and outside the main coil. To confirm this experimentally, we measured a nutation curve of a rotor where the sample was restricted by PTFE spacers to the volume inside the main coil (center 2.5 mm of the 5.3 mm long cylindrical sample space in the rotor). Indeed only the low-field part of the distribution of B_1 fields was observed. It is important to note that this inhomogeneity of the ^{2}H field does not deteriorate the decoupling performance in practice, because the part of the sample that experiences the higher ^{2}H B_1 field is outside the main coil and is not detected in most experiments, not only because of the lower detection sensitivity but also because of inefficient excitation and polarization transfer for this part of the sample.

To allow decoupling also during proton detection (which turns out to be unnecessary in our experiments) we checked whether the rf on the ^{2}H coil is picked up by the main coil, i.e. whether ^{2}H decoupling creates noise in the ^{1}H dimension. However, the noise level in the ^{1}H FID with and without ^{2}H decoupling is identical, indicating that ^{2}H decoupling can be applied also during detection. We also investigated the possible impact of the additional coil on the performance of the main resonance circuit by testing rf fields and detection sensitivity on an alanine test sample before and after installation of the ^{2}H coil. On the ^{13}C channel, the power level for 100 kHz and the detection sensitivity remained unchanged. The ^{1}H resonance frequency of the main coil decreased by about 5 MHz upon installation of the ^{2}H coil, most likely due to parasitic capacitances. To allow tuning it to the Larmor frequency, the length of the transmission line was adjusted by sliding the telescope-like inner conductor slightly together. The power requirement of the ^{1}H channel increased by 2 dB and concurrently the detection sensitivity dropped by 15%, which is however significantly less than the gain due to the ^{2}H decoupling with the installed ^{2}H coil.

We then tested the decoupling performance by collecting 2D[^{13}C,^{1}H]-HSQC correlation spectra on a microcrystalline sample of the protein ubiquitin labeled with $^{13}CHD_2$ groups on Isoleucine-δ_1 positions, and perdeuterated otherwise. We focus here on proton-detected spectra of these methyl groups. The one-bond scalar coupling between deuterium and carbon, $^1J_{CD}$ is approximately 20 Hz [11], and without decoupling the presence of two ^{2}H nuclei gives rise to a quintet of lines with 1:2:3:2:1 intensity ratio, separated by the scalar coupling constant. The scalar coupling to the proton, $^2J_{HD}$, is much smaller, on the order of 2 Hz. We, thus expect that scalar decoupling of ^{2}H greatly reduces line widths of ^{13}C, while the effect on a ^{1}H dimension should be much smaller. Fig. 4 shows experimental data of these methyl groups in the presence of a 2 kHz WALTZ decoupling field during the indirect ^{13}C dimension

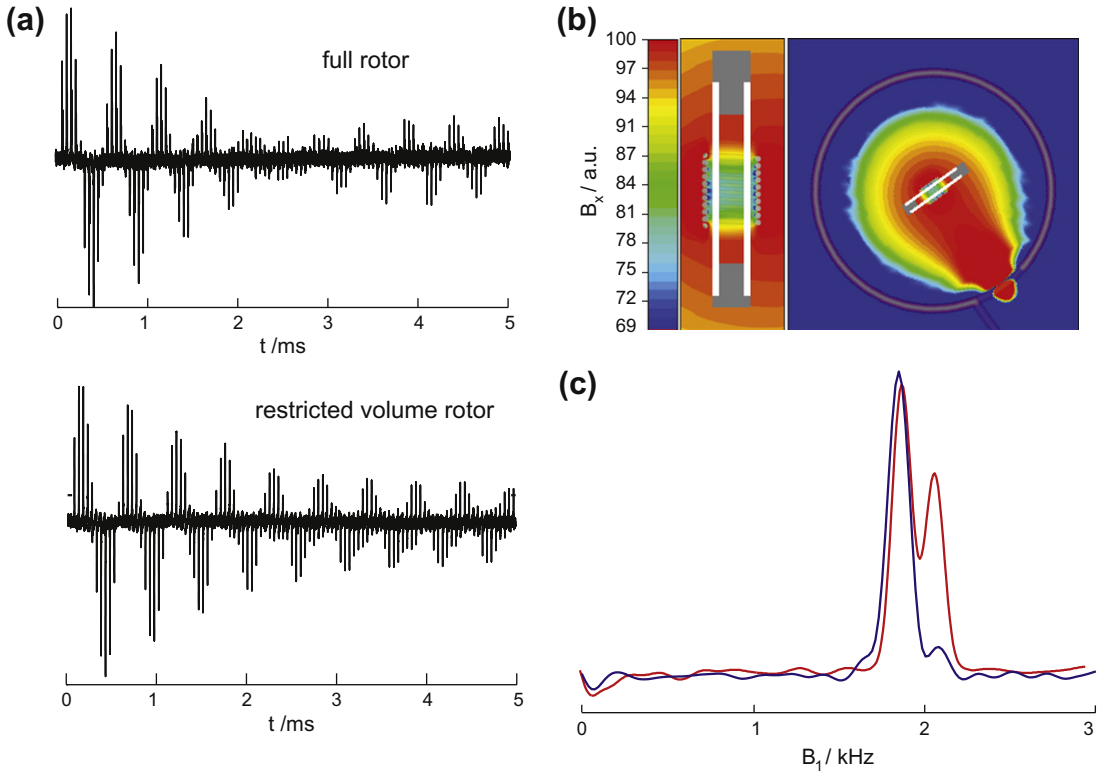

Fig. 3. B_1 field strenght and homogeneity induced in the sample by the external ^{2}H coil. (a) Stack plot of 1-pulse ^{2}H experiments as a function of pulse length. (b) Finite-element simulated B_1 field distribution. On the right, a zoom on the 1.3 mm rotor inside the regular solenoid coil. (c) B_1 field strengths from the nutation experiment of the full rotor (red) and with the sample restricted to the volume inside the inner coil (blue). The 810°/90° ratio is 67%.

(red) and without ^{2}H decoupling. In all cases, the carbon-proton coupling was eliminated, either by a π pulse applied to protons during ^{13}C chemical-shift evolution, or by 2.5 kHz ^{13}C WALTZ decoupling during ^{1}H detection. The improvement in ^{13}C line width provided by the ^{2}H decoupling is shown by ^{13}C FID data (Fig. 4a) and frequency domain data (Fig. 4b and c). Without decoupling ^{13}C linewidths are 58 ± 6 Hz (the $^1J_{CD}$ multiplet structure is not resolved), with decoupling they decrease to 21 ± 3 Hz. The peak intensity increases by a factor of 2.8 ± 0.5. This corresponds to a sensitivity gain of a factor 2.4 taking into account the 15% loss of ^{1}H sensitivity upon installation of the ^{2}H coil. This improvement indeed greatly accelerates data acquisition (by about a factor of 5.5 (i.e. 2.4^2) for a 2D spectrum, and a factor of 30 when methyl–methyl cross peaks are recorded, as in the context of structure determination [5]). We also tried applying ^{2}H decoupling during ^{1}H acquisition but did not observe an improvement in linewidth because other factors dominate.

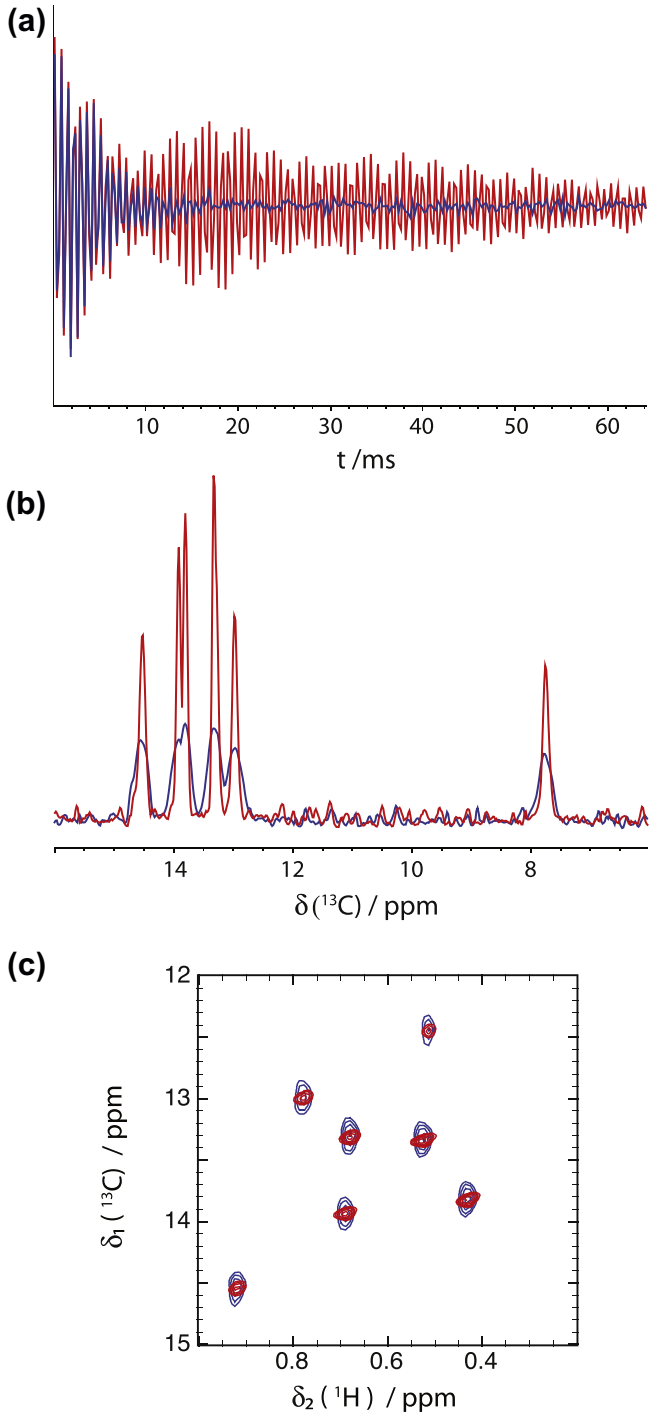

Fig. 4. Effect of decoupling with the external ^{2}H coil observed on [U-^{2}H,^{15}N, Ile–^{13}CHD$_2$] labelled ubiquitin microcrystals at 55 kHz MAS. (a) Indirect ^{13}C FID extracted at the ^{1}H frequency of Ile 3 from a proton-detected HSQC experiment with 2 kHz ^{2}H WALTZ decoupling (red) and without (blue). (b) Projection of the resulting spectrum on the ^{13}C axis. (c) Overlay of the decoupled and not decoupled [^{13}C;^{1}H]-HSQC spectra. The peak at $\delta^{13}C \approx 8$ ppm in b) is aliased in this spectrum. The acquisition time for the 2D data set was 3 h. The decoupled peaks are slightly skewed due to correlated inhomogeneous broadening.

In solution-state NMR the ^{2}H circuit it typically used for field locking and decoupling. We used the auxiliary coil only for decoupling. Tests with a 3.2 mm probe and the main coil tuned to ^{2}H have shown that it is possible to lock on the D_2O line of microcrystalline protein samples but the sensitivity of the external coil is too low for this to be practical with a 1.3 mm rotor. Furthermore locking on the D_2O resonance with fast magic-angle spinning (50 kHz in this case) carries the risk of correcting for shifts that are actually due to thermal effects and not a change in the B_0 field.

4. Conclusions

We have shown that an auxiliary ^{2}H coil outside of the MAS stator can be used for ^{2}H decoupling in partially deuterated proteins, which greatly increases peak intensity and resolution. Deuterium-detection sensitivity is sufficient for easy calibration of the decoupling power level through a nutation experiment and direct ^{2}H detection. The presented analytical and numerical calculations correctly predict the magnitude of the observed B_1 field as well as the form and origin of the inhomogeneity.

5. Experimental methods

All NMR experiments were carried out on a Bruker Biospin AVANCE II + spectrometer operating at 850 MHz ^{1}H frequency using a 1.3 mm triple-resonance (^{1}H,^{13}C,^{15}N) probe (Bruker).

The conductors (silver-plated copper wire, diameter 1 mm) of the auxiliary ^{2}H coil were wound around PTFE disks, which are placed on the side of the stator. The tuning elements were placed below the stator chamber. The connecting coaxial cable was guided through a preexisting hole with the shield connected to the probe's frame at several points to achieve good grounding.

Finite elements simulation of the B_1 field was performed with CST Microwave Studio 2010 using the time domain transient solver. The magnetic field was simulated at a fixed input current with minimum mesh size of 0.05 mm.

[U–^{2}H^{15}N; Ile–^{13}CD$_2$H] ubiquitin was produced and crystallized as described in [5] with the exception that 4-^{13}CHD$_2$-3-d$_2$-α-ketobutyrate (75 mg/L, Sigma) was added to the bacterial medium instead of α-ketoisovalerate.

[^{13}C; ^{1}H] HSQC spectra shown in Fig. 4 were with 512 t_1 increments and 16 scans, leading to an experimental time of 3 h for each spectrum. B_0 drift (maximally 20 Hz) was corrected by applying a "first order phase correction" on the ^{1}H free induction decay leading to a frequency shift in the spectrum. The angle was increased linearly between different t_1 traces.

Acknowledgments

This work was supported by the Swiss National Science Foundation (Grant 200020_134681) and the European Commission under the Seventh Frame- work Programme (FP7), contract Bio-NMR 261863.

References

[1] S. Asami, P. Schmieder, B. Reif, High resolution ^{1}H-detected solid-state NMR spectroscopy of protein aliphatic resonances: access to tertiary structure information, J. Am. Chem. Soc. 132 (2010) 15133–15135.

[2] V. Chevelkov, K. Rehbein, A. Diehl, B. Reif, Ultrahigh resolution in proton solid-state NMR spectroscopy at high levels of deuteration, Angew. Chem. Int. Ed. 45 (2006) 3878–3881.

[3] V. Agarwal, A. Diehl, N. Skrynnikov, B. Reif, High resolution H-1 detected H-1, C-13 correlation spectra in MAS solid-state NMR using deuterated proteins with selective H-1, H-2 isotopic labeling of methyl groups, J. Am. Chem. Soc. 128 (2006) 12620–12621.

[4] N.K. Goto, K.H. Gardner, G.A. Mueller, R.C. Willis, L.E. Kay, A robust and cost-effective method for the production of Val Leu Ile (delta 1) methyl-protonated N-15-, C-13-, H-2-labeled proteins, J. Biomol. NMR 13 (1999) 369–374.

[5] M. Huber, S. Hiller, P. Schanda, M. Ernst, A. Böckmann, R. Verel, B.H. Meier, A. Proton-Detected, 4D solid-state NMR experiment for protein structure determination, Chem. Phys. Chem. 12 (2011) 915–918.

[6] B. Reif, Y. Xue, V. Agarwal, M.S. Pavlova, M. Hologne, A. Diehl, Y.E. Ryabov, N.R. Skrynnikov, Protein side-chain dynamics observed by solution – and solid-state NMR: comparative analysis of methyl H-2 relaxation data, J. Am. Chem. Soc. 128 (2006) 12354–12355.

[7] P. Schanda, M. Huber, J. Boisbouvier, B.H. Meier, M. Ernst, Solid-state NMR measurements of asymmetric dipolar couplings provide insight into protein side chain motion, Angew. Chem. Int. Ed. (2011).

[8] A.J. Shaka, J. Keeler, Broadband spin decoupling in isotropic liquids, Prog. NMR Spectrosc. 19 (1987) 47–129.

[9] J. Mispelter, M. Lupu, A. Briguet, NMR probeheads for biophysical and biomedical experiments: theoretical principles & practical guidelines, Imperial College Press, London, 2006.

[10] R.S. Elliott, IEEE antennas and propagation society electromagnetics: history theory and applications, IEEE Press, Piscataway, NJ, 1993.

[11] M. Alei Jr, W.E. Wageman, Gas phase C chemical shifts and coupling constants in the deuteromethanes, J. Chem. Phys. 68 (1978) 783.